Columnar phase structures of an organic–inorganic hybrid functionalized with eight calamitic mesogens†

Panagiota K. Karahaliou,*[a] Paul H. J. Kouwer,[b] Thomas Meyer,[b] Georg H. Mehl[b] and Demetri J. Photinos[a]

Received 5th December 2006, Accepted 21st March 2007
First published as an Advance Article on the web 17th April 2007
DOI: 10.1039/b617696h

A liquid-crystalline octapode, formed by laterally connecting calamitic mesogens to an inorganic silsesquioxane cube through flexible siloxane spacers, is studied using polarized light microscopy, differential scanning calorimetry (DSC) and X-ray diffraction (XRD). The studies are extended to mixtures of the octapode with the respective monomer mesogens. The monomer and the octapode show a nematic phase. At lower temperatures, the octapode exhibits additionally a columnar hexagonal phase (*p6mm* lattice), which, on further cooling, undergoes a transition to a columnar rectangular phase (*p2gg* lattice). A similar phase-transition sequence is observed for mixtures of the octapode with moderate concentrations of the monomer. The columnar–columnar transition is discussed combining XRD and DSC results, and a possible model of the molecular self-organization is presented.

Introduction

The self-organization of functional supermolecular structures, such as oligomers, dendrimers and hyperbranched polymers,[1–8] into thermotropic liquid-crystalline materials is increasingly attracting attention. A basic advantage of these new materials is the controllability of their size and architecture and thus of their physicochemical properties.

Supermolecular mesogens typically consist of a number of conventional mesogens linked to a supermolecular core according to a specific architecture (dendritic, hyperbranched *etc.*). They tend to show a rich variety of mesophases whose formation is driven by the interplay between the shape of the individual mesogens and the structure of their supermolecular assembly. These molecular features are the basis of the two main mechanisms by which mesomorphic ordering is formed, namely by steric constraints in the molecular packing and by micro-segregation among chemically different molecular segments.[9–11] The mesomorphic behavior of these systems shows certain striking differences from that of simple "monomeric" mesogens. On a molecular level, these differences are thought to stem from the configurational correlations that the connectivity of the supermolecular assembly imposes on the mesogenic units. Within a given architecture, such correlations can be controlled to some extent by chemically varying certain structural parameters, primarily branch length, mesogen grafting-density and dendritic generation.

For mesogenic dendrimers of relatively low generation and with sufficiently long and flexible branches, it is known that the ordering is essentially dictated by the aligning tendency of the mesogenic units in conjunction with their tendency to micro-segregate away from the flexible branches.[12] In contrast, the behavior of densely, and therefore tightly, connected mesogenic units is more complex as it is additionally influenced by the global orientability of the supermolecular assembly.[9,13] Accordingly, a richer mesomorphism is expected.[7,14,15] Supermesogenic compounds based on the silsesquioxane cube are suitable for studying such mesomorphism because they reach the dense packing limit at early generations. Here we report on structural studies of octapodes formed by conventional low molar mass molecules laterally linked to a silsesquioxane cube. X-Ray diffraction (XRD) is used for the structural investigation of the self-organization of these compounds. The studies are extended to binary mixtures of the octapodes with the monomeric compound in order to elucidate the influence of increasing the total mesogen volume-fraction in the system.

Experimental

The octapodes are formed by lateral substitution of the mesogenic groups to the inorganic silsesquioxane cube through identical flexible spacers, each consisting of five methylene units and a siloxane group, as shown in Fig. 1a. The mesogenic side-groups are denoted as $\mathbf{B_1}$ and the octapode as compound **C-8B**. The details of the synthesis have been reported earlier and follow a typical approach, where the inorganic core and a functionalized mesogen are coupled in a final hydrosilylation reaction.[16] Fig. 1b shows the precursor **B**. The synthesis of mesogen **B** has been described elsewhere.[17]

In addition to the pure compounds, XRD results are reported for mixtures of mesogen **B** with octapode **C-8B** (denoted as **B÷C-8B**) at three different concentrations x. For convenience, the concentration throughout this paper is defined as the ratio of the number of mesogenic side-groups assembled into octapodes over the total number of mesogenic units in the mixture (see Appendix1). Three different mixtures were investigated, 1 : 1 (w/w), 3 : 1 (w/w) and 7 : 1 (w/w). These correspond to concentrations of x = 0.44, 0.69 and 0.84, respectively.

[a]*Department of Materials Science, University of Patras, 26504, Patras, Greece. E-mail: pkara@upatras.gr*
[b]*Department of Chemistry, University of Hull, Hull, HU6 7RX, UK*
† The HTML version of this article has been enhanced with colour images.

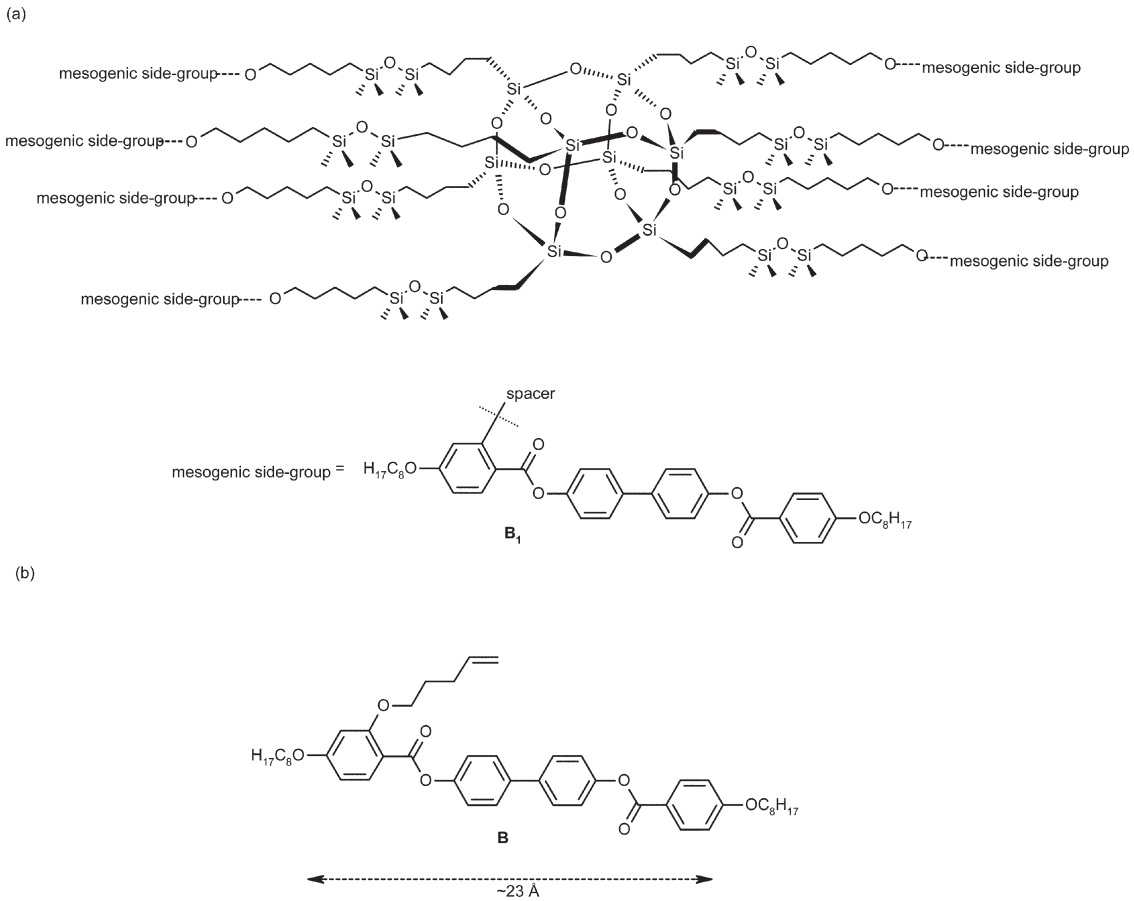

Fig. 1 (a) Octapodes formed by lateral attachment of mesogenic side-groups $\mathbf{B_1}$ to the inorganic cube through a flexible spacer. (b) Mesogens **B**. The length of the aromatic core of **B** (same as $\mathbf{B_1}$) is indicated.

Phase transitions were determined using a Perkin-Elmer DSC 7 under a nitrogen atmosphere against an indium standard. Transition temperatures correspond to the onset of the exotherm of each transition, during the cooling cycle (cooling rate 10 °C min^{-1}). The mesophases were studied on an Olympus BH-2 optical polarizing microscope (POM), equipped with a Mettler FP82 HT hot stage, a Mettler FP90 central processor and a JVC digital video camera. XRD experiments were performed on a MAR345 diffractometer with a 2D image-plate detector (CuKα radiation, graphite monochromator, λ = 1.54 Å). The samples were heated in the presence of a magnetic field using a home-built capillary furnace. The data sets were analysed using the "FIT2D" software package available from the ESRF, Grenoble, France and Origin Pro7 software package from OriginLab.

Results

Liquid-crystal temperature ranges

The mesomorphic ranges and transition enthalpies of the compounds and mixtures are summarized in Table 1. All the compounds and mixtures studied here show a nematic phase.

The octapode **C-8B** undergoes a nematic to columnar hexagonal phase transition. Further cooling leads to the formation of a columnar rectangular phase. The transition temperatures are similar to those reported in ref. 18. It should be noted, however, that the provisional assignment of the low temperature, higher ordered LC phases, which was based on optical polarizing microscopy,[18] had to be revised. Indeed the ambiguity of this initial phase assignment was a motive for the present investigation. For dendrimers based on the same

Table 1 Liquid-crystal temperature ranges and transition enthalpies of pure compounds and binary mixtures

Substance	Phase sequence T/°C (ΔH/kJ mol^{-1})[a]	$\Delta H_{NI}\langle n\rangle^{-1}$ [b]/kJ mol^{-1}
C-8B	Cr 46 (31.8) Col_r 92[c] Col_h 109.5 (3.0) N 143 (12.1) Iso	1.5
B÷**C-8B** (x = 0.84)	Col_r 31 (16.5) Col_h 81 (12.1) N 144 (11.3) Iso	1.2
B÷**C-8B** (x = 0.69)	Col_r 10[c] Col_h 68 (12.1) N 145 (11.1) Iso	1.0
B÷**C-8B** (x = 0.44)	Cr 20 (75.8) Col_h 31 (9.1) N 152 (16.7) Iso	0.9
B	Cr 98 (32.6) N 173 (1.8) Iso	1.8

[a] Details for the calculation of the transition enthalpies in kJ mol^{-1} are given in Appendix 2 [b] Latent heat at the nematic to isotropic transition, normalized per mesogenic group in the system. [c] Transition enthalpies are not reported due to weak and broad exotherms associated with the Col_r–Col_h phase transition

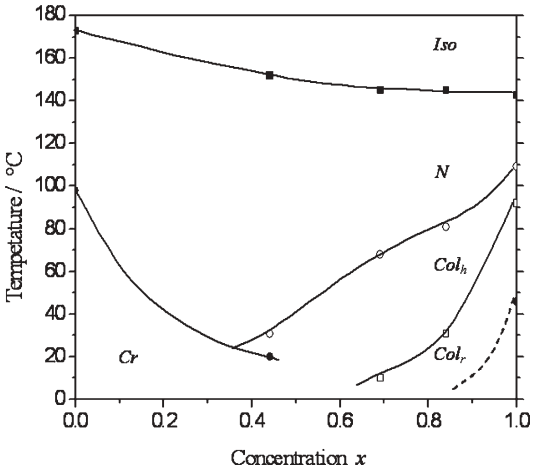

Fig. 2 Temperature–concentration phase diagram for the mixtures of **B**÷**C-8B**.

mesogen, a tilted columnar phase was detected.[19] Other experimental results, concerning classical calamitic mesogens forming columnar structures in supermolecular systems, also indicate[7] that optical defect textures for higher ordered LC phases are potentially unreliable.

The phase behavior of the mixtures as a function of concentration is shown schematically in Fig. 2. These results are based on POM studies of the compounds and of the specific binary mixtures listed in Table 1. For confirmation purposes, the characteristic textures (Fig. 3) observed for these systems were also identified in POM observations on contact samples of **B** and **C-8B**.

It is evident from the phase diagram in Fig. 2, that the nematic to isotropic transition temperature remains nearly constant over most of the concentration range. The range of the two low temperature columnar phases shifts to lower temperatures with increasing monomer concentration. In other words, the addition of monomer destabilizes the higher ordered LC phases. The Col_h and the Col_r phases disappear somewhat below the concentrations of 0.44 and 0.69, respectively.

XRD results

The diffraction patterns of **C-8B**, taken at three different temperatures (140, 107 and 62 °C), corresponding to the nematic, the columnar hexagonal and the columnar rectangular phase,

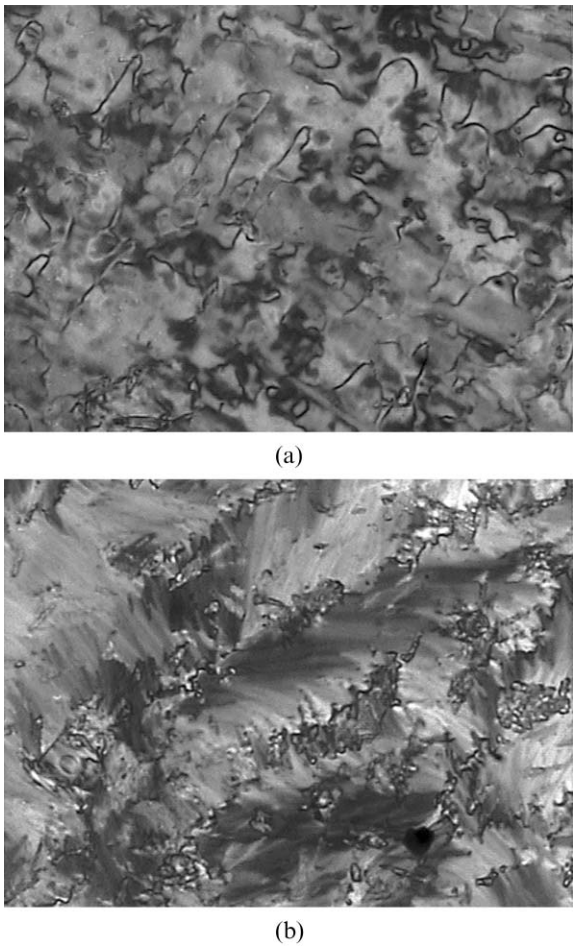

Fig. 3 POM images of the mesophases of compound **C-8B**. (a) Nematic phase at 135 °C, (b) Col_h phase at 107 °C.

are shown in Fig. 4. The typical diffuse diffractions at wide angles, corresponding to the silicon groups ($2\pi/q \approx 6$ Å) and to the hydrocarbon chains ($\approx$4.5 Å), were observed in all three mesophases, in accordance with their liquid-like structure. The radially and azimuthally integrated diffraction intensities for the entire temperature range of the experimental study are shown in Fig. 5a and 5b.

Notable are the four, small-angle, off-meridian, intensities in the nematic phase. Similar off-meridian reflections were observed in the nematic phase of the monomer **B**. Four-spot reflections in a nematic phase have been long known[20] and are

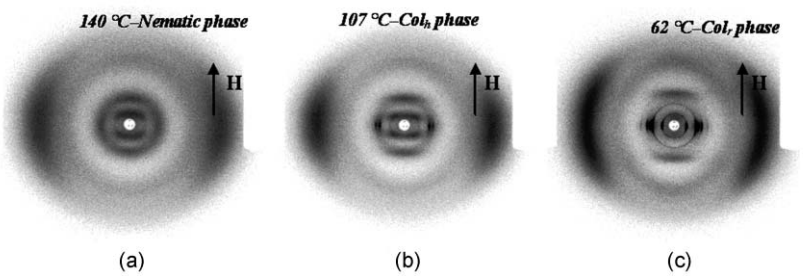

Fig. 4 Representative 2D-diffraction patterns of the octapode **C-8B** in the nematic (a), Col_h (b) and Col_r (c) phase. The arrows indicate the direction of the magnetic field H.

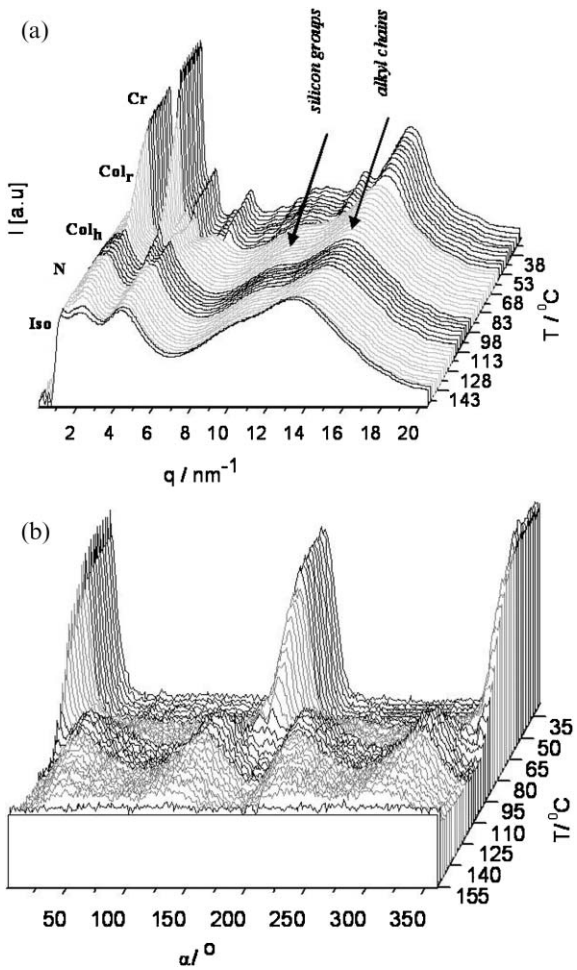

Fig. 5 (a) Radially integrated diffraction intensities as a function of temperature T and of wave-vector magnitude q for the octapode **C-8B**. (b) The respective azimuthally integrated diffraction intensities as a function of temperature T and azimuth angle α.

usually attributed to the formation of SmC-like cybotactic clusters, *i.e.* locally tilted layered structures immersed in a normal nematic matrix. The appearance of such reflections has often been observed in nematic phases formed by molecules of various architectures: main-chain polymers,[21] side-chain polymers with laterally[22] as well as with longitudinally[23] attached mesogenic units, dendrimers[3] and bent-core mesogens.[24] An analogous interpretation in terms of cybotactic clusters is possible for the four pseudo-Bragg-like reflections observed in the nematic phase of the systems in the present work. However, the surprising result of this study is the persistence of the four-spot reflection in the Col$_h$ phase in the case of the pure octapode **C-8B** as well as in the case of the **B**÷**C-8B** ($x = 0.69$) mixture. To our knowledge, this is the first time that a molecular organization in tilted layers has been observed in a columnar phase of calamitic mesogens. Columnar phases formed by calamitic molecules that are possibly stacked obliquely with respect to the column axis have been reported previously;[25] these are not to be confused with the tilted arrangements described here, where the calamitic units are parallel to the columnar axis but they form "slices" that are obliquely stacked with respect to the columnar axis.

In addition to the off-meridian reflections, notable is the presence of a diffuse peak on the meridian in the hexagonal phase. An analogous peak, albeit shifted to higher values of the wave vector, is also observed in the Col$_r$ phase. These diffuse peaks are attributed to the stacking of the silsesquioxane cubes and give the average distance between two cubes in a column. Finally, all the peaks located on the equator of the diffractograms in the hexagonal and the rectangular phase can be identified with the characteristic spacings of a hexagonal (*p6mm*) and a rectangular (*p2gg*) lattice, respectively. The analysis of the diffractograms for the two columnar phases is presented below.

The columnar hexagonal phase

The diffraction pattern taken from the high temperature Col$_h$ phase of the octapode **C-8B** is given in Fig. 6a. The radially integrated intensities, over the meridian and equatorial sectors indicated in Fig. 6a, are plotted in Fig. 6b. Integration in sectors is used in order to separate diffractions recorded on the equator (perpendicular to the magnetic field) from the ones recorded on the meridian (parallel to the field). In these

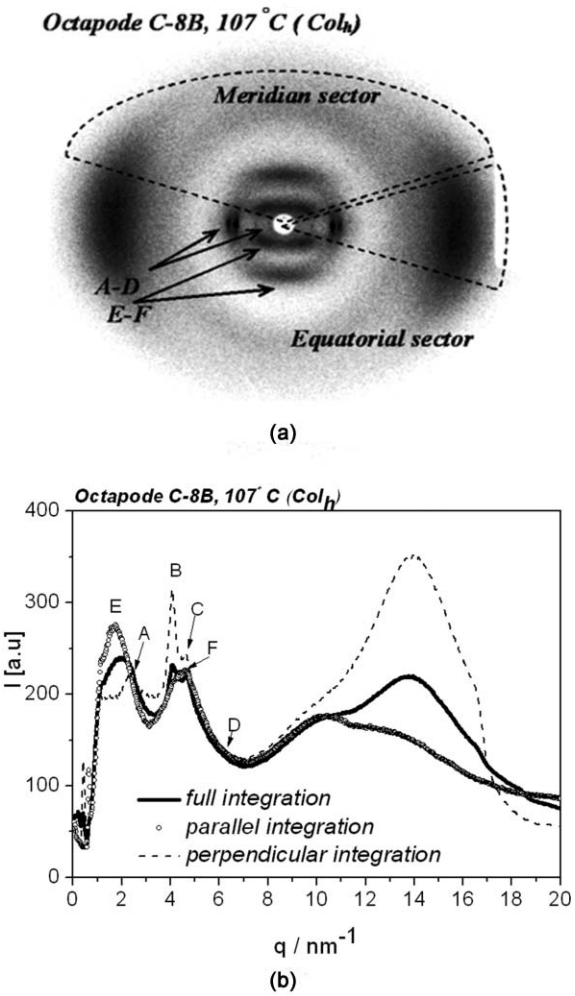

Fig. 6 2D diffraction pattern (a) and radially integrated diffraction intensities (b) for the octapode **C-8B** in the Col$_h$ phase at 107 °C.

Table 2 Experimentally determined values of spacings d_{hk} for the Col_h phase, as obtained directly from the reflections A–F shown in Fig. 6, at 107 °C for the octapode **C-8B**. The values in parentheses are obtained by fitting the experimental reflections to a 2D hexagonal lattice

Peak	A	B	C	D	E	F
hk	10	11	20	21	—	—
d_{hk}/Å	26.7 (27.0)	15.5 (15.6)	13.6 (13.5)	10.3 (10.2)	36.40	14.04

integrations, a normalization with respect to the sector aperture is applied, and therefore the direct addition of the normalized intensities of the two sectors does not give the fully integrated intensity. Moreover, as the relative apertures assigned to these sectors are to some extent arbitrary, some arbitrariness is carried over to the relative intensities of some of the peaks in Fig. 6b. Thus, for example, the relative intensities of peaks A and B could be changed by decreasing the aperture of the parallel integration over the perpendicular one. Accordingly, unambiguous comparisons of peak intensities are strictly possible only for the fully integrated intensities.

The recorded intensities on the equator correspond to the 2D hexagonal lattice (peaks A–D in Fig. 6). The reflections on the meridian or close to it (E and F in Fig. 6) originate from the mesogenic groups and the silsesquioxane cubes. Peak F is attributed to the intra-columnar cube–cube stacking. Peak E, at 36.40 Å, corresponds to the four–spot, off–meridian reflections.

Reflections A–D in the diffraction pattern of Fig. 6a are of ratios very close to $1 : \sqrt{3} : 2 : \sqrt{7}$, characteristic of a 2D hexagonal lattice. By fitting the experimental reflections of **C-8B**, **B**÷**C-8B** (x = 0.84) and **B**÷**C-8B** (x = 0.69) to a 2D lattice, we determine the spacings d_{hk} (Table 2) together with the lattice constant a, (Table 3).

From the experimentally determined lattice constants, we obtain the unit-cell surface area S_u. The experimental value of the stacking distance h_c of the silsesquioxane cubes within a column is obtained from the d spacing of the reflection F on the meridian. The diffuse appearance of the reflection F in the diffractogram indicates the high degree of disorder in the intra-columnar stacking.

The experimentally determined average molecular volume V_m per cube of the **C-8B** octapode is given by:

$$V_m = h_c S_u, \quad (1)$$

Based on the assumption that one molecule can fill the cross-sectional area of the column, the mass density ρ of the compound is related to V_m through the molar mass M according to:

$$\rho = M/N_A V_m. \quad (2)$$

This leads to the density evaluation shown in Table 3.

For the molecular volume V_m per cube of the **B**÷**C-8B** mixtures, proper account is taken of the added monomers. The quite reasonable results found for the mass density in Table 3, $\rho \approx 10^3$ kg m^{-3}, support the molecular packing scheme assumed for the hexagonal columnar phase.

The columnar rectangular phase

The transition from the columnar hexagonal to the rectangular phase is associated with a noticeable change in the diffraction patterns (compare Fig. 4b and Fig. 4c). An analysis along similar lines with the columnar hexagonal phase was carried out to identify and separate the different reflections parallel and perpendicular to the magnetic field. Reflections A–F in Fig. 7a, are attributed to the non-centered rectangular lattice, (in this sense, they are the counterparts of the reflections labeled A–D of the high temperature hexagonal phase). The diffuse peak, labeled G, on the meridian in the diffractogram shown in Fig. 7a is the counterpart of peak F found in the hexagonal phase.

The radial integrations are given in Fig. 7b and the calculated spacings d_{hk} are listed in Table 5. The sufficient number of reflections makes it possible to recognize a *p2gg* rectangular lattice. The lattice constants a, b in Table 4 were determined by fitting the reflections found experimentally to a two-dimensional monoclinic cell. In a *p2gg* phase-symmetry, reflections (h0) and (0k) with odd h and k are forbidden. Some reflections are found to be superposed (see Table 4). The unit cell contains two columns, compared to the single column in the Col_h unit cell. In this non-centered Col_r phase, the effective cross-section of the columns becomes elongated, with long axes in alternating directions.

Packing density considerations analogous to those presented for the columnar hexagonal phase are used for the calculation of the molecular volume per silsesquioxane cube in the sample and of the mass density in the Col_r phase. In both, the pure **C-8B** octapode and the **B**÷**C-8B** (x = 0.84) mixture, the surface area of the unit cell is found to be more than twice the surface area of the hexagonal phase. Accordingly, the surface area per column S_c, which is half of the unit cell area, is slightly larger than the area per column in the hexagonal phase. This increase goes along with a slight decrease in the calculated cube-stacking distance. The results are summarized in Table 5. The experimentally defined molecular volume V_m per cube and the calculated mass density $\rho \approx 10^3$ kg m^{-3}, are very close to the respective values found for the hexagonal phase and confirm the validity of the molecular packing assumed for the rectangular columnar phase.

It is worth noting in Table 4 that the (20) and (11) peaks coincide. This means that the a/b ratio is exactly $\sqrt{3}$, which is

Table 3 Hexagonal lattice constant a, unit-cell surface area S_u, stacking periodicity (the distance between two successive cubes in a column) h_c, molecular volume V_m per silsesquioxane cube in the sample and mass density ρ, evaluated according to Eqn (2), for the Col_h phase of the pure **C-8B** compound and of the **B**÷**C-8B** mixture at two concentrations

Substance	T/°C	a/Å	10^3 S_u/Å^2	h_c/Å	10^3 V_m/Å^3	ρ/kg m^{-3}
C-8B	107	30.95	0.83	14.04	11.65	1080
B÷**C-8B** (x = 0.84)	80	33.07	0.95	14.29	13.57	1064
B÷**C-8B** (x = 0.69)	26	34.84	1.05	14.55	15.28	1095

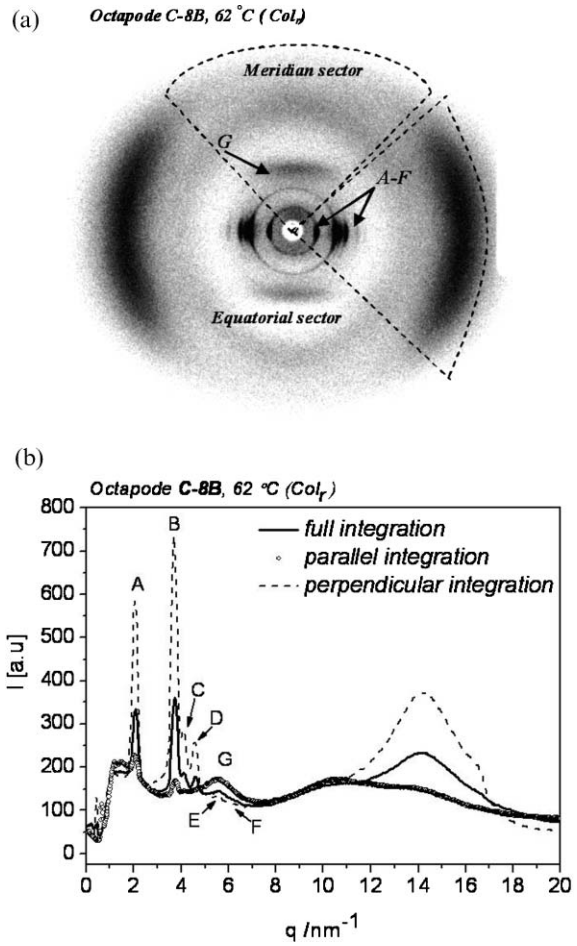

Fig. 7 2D diffraction pattern (a) and radially integrated diffraction intensities (b) of the octapode **C-8B** in the Col_r phase at 62 °C.

the value for the Col_h phase when a centred rectangular unit cell is used. Furthermore, some low-index diffraction peaks, such as (02), (21), (31), are missing from the experimental diffraction pattern. While the above features are not impossible for a *p2gg* lattice, one may wonder if an alternative indexing of the phase with a higher symmetry, *e.g. c2mm*, could be possible. To address this possibility, we have fitted the experimental values of the spacings d_{hk} to a *c2mm* lattice, where symmetry allows only reflections corresponding to even values of $h + k$. The overall quality of these fits is not inferior to that of the *p2gg* fits. Moreover, some low-index diffraction peaks, notably the (11) peak, turn out to be missing from the experimental diffraction pattern according to the *c2mm* indexing. Thus, the experimental resolution is not sufficient to single out one of the two symmetries by directly fitting the diffraction pattern. However, considerations based on the very small enthalpy of the observed Col_h–Col_r phase transition are clearly in favour of a *p2gg* symmetry: (a) the unit cell obtained for the *c2mm* lattice implies a density increase of at least 10% at the transition, such a large increase would not be justified by the small enthalpy of the transition; (b) the *p2gg* symmetry, being closer to the symmetry of the hexagonal phase, is in better accordance with the weakness of the phase transition.

Discussion

It is apparent from the temperature–concentration phase diagram of Fig. 2 that increasing the concentration of the low molar mass mesogens eventually leads to the disruption of the columnar ordering. This clearly shows that the columnar ordering is not due to the direct self-organization of the individual calamitic units but rather to their assembly into octets (*via* their lateral attachment to the silsesquioxane cubes). The question of how the low molar mass mesogens are incorporated into the columnar structures remains to be addressed. To this end, two possibilities are considered: (a) the low molar mass mesogens could be located mainly in the inter-columnar space, *i.e.* between mesogenic octapodes belonging to adjacent columns. With increasing monomer concentration in the mixtures, this would lead to an increase of the columnar lattice constants, without directly affecting the stacking periodicity along the columnar axis. In an extreme case, this mechanism would lead to columns surrounded by a sheath of low molar mass mesogens; (b) alternatively, the low molar mass mesogens might be inserted into the columnar assembly. In this case, an increase of their proportion in the mixture would lead to an increase of the distances between LC octapodes within a column and to only a small expansion of the columnar lattice.

The XRD results presented in Table 3 show that, in the columnar hexagonal phase, the addition of low molar mass

Table 4 Experimentally determined values of spacings d_{hk}, for the Col_r phase, as obtained directly from the reflections A–G shown in Fig. 7, at 62 °C for the octapode **C-8B**. The values in parentheses are obtained by fitting the experimental reflections to a 2D rectangular lattice

Peak	A	B	C	D	E	F	G
hk	20, 11	12	40, 22	41	13, 42, 51	52	—
d_{hk}/Å	30.5 (30.5)	16.9 (16.9)	15.3 (15.2)	13.7 (14.0)	11.3 (11.5)	10.0 (10.0)	11.30

Table 5 Lattice constants a and b, surface area per column S_c (half of the unit-cell surface area), stacking periodicity (the distance between two successive cubes in a column) h_c, molecular volume V_m per silsesquioxane cube in the sample and mass density ρ, evaluated according to Eqn (2), for the Col_r phase of the pure **C-8B** system and of the mixture **B÷C-8B** (x = 0.84)

Substance	T/°C	Lattice constants	$10^3\ S_c$/Å^2	h_c/Å	$10^3\ V_m$/Å^3	ρ/kg m^{-3}
C-8B	62	a = 60.9 Å; b = 35.2 Å	1.07	11.30	12.10	1040
B÷C-8B (x = 0.84)	56	a = 60.0 Å; b = 34.7 Å	1.04	13.50	14.00	1027

mesogens leads to an increase of both the hexagonal lattice constant and the stacking periodicity along the columnar axis, suggesting that both possibilities (a) and (b) might be operative. However, the XRD results for the columnar rectangular phase, presented in Table 5, show that the addition of low molar mass mesogens leads to a substantial increase of the stacking periodicity along the columnar axis without appreciable changes of the rectangular lattice constants. This suggests that possibility (b) dominates in the columnar rectangular phase. Moreover, one might speculate that the above differences in the packing of the mesogenic units around the columns in the two phases underlie the observation of a tilted ordering in the hexagonal phase but not in the rectangular.

A molecular model is proposed for the interpretation of the structural XRD results:

(i) In the nematic phase of the **C-8B** octapode, the director is oriented parallel to the magnetic field while the mesogenic side-groups are arranged in SmC-like cybotactic clusters, whose size is of the order of a few nanometres. The cybotactic layer-normals are tilted with respect to the magnetic field. The respective tilt angle is found to attain values as high as 50°.

(ii) A possible molecular organization scheme for the Col_h phase is shown in Fig. 8a and Fig. 8b. Here too, the director associated with the mesogenic side-groups is oriented parallel to the magnetic field and to the long columnar axis. The column formation results from the microsegregation between the silsesquioxane and the mesogenic parts. The silsesquioxane cubes and the spacers form the columnar interior, around which the mesogens are evenly distributed to form the outer shell of the column. Accordingly, the mesogens from one octapode can interact with neighbours within the same or adjacent columns. The cybotactic tilt implies a tilted arrangement of the pseudo-layers formed by the mesogens in the outer columnar shell. Considering the length of the mesogen aromatic core (23 Å), the average stacking distance between the two silsesquioxane cubes (14 Å) implies that the mesogenic side-groups from successive octapodes along a column are interdigitated by less than a half of their length.

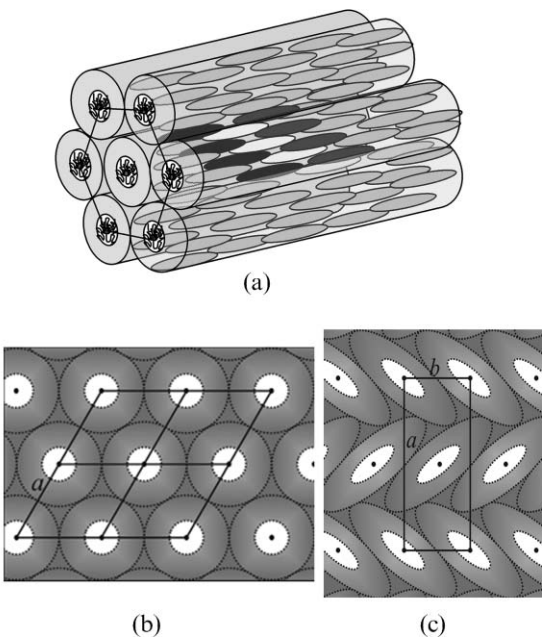

Fig. 8 Possible molecular self-organization of the **C-8B** octapodes in the columnar phases. (a) Side view of the Col_h phase. The different filling (black, white, dark grey) is meant to distinguish between mesogenic side-groups attached to different silsesquioxane cubes situated successively along the same column. (b) Top view of the hexagonal lattice. Grey and white parts represent, respectively, regions with a high density of mesogenic groups and regions with a high density of silsesquioxane cubes and spacers. (c) Top view of the rectangular lattice in the Col_r phase.

(iii) Fig. 8b represents a top view of the hexagonal lattice. Two distinct areas can be identified. The silsesquioxane cubes and the lateral spacers occupy the inner part of the column. This part is surrounded by the mesogenic side-groups. The suggested molecular organization scheme satisfies both the microsegregation of chemically different molecular species and the rotational symmetry within the column, according to which the columnar axis in the Col_h phase is an axis of rotational symmetry and the mesogenic side-groups are, on average, distributed uniformly around this axis.

(iv) The transition from the Col_h to the Col_r phase is accompanied by the symmetry change from a *p6mm* to a *p2gg* lattice. The distance between the silsesquioxane cubes decreases to 11.3 Å and the columnar cross-section increases to 1070 $Å^2$. The rotational symmetry within the column is lost. Accordingly, the columnar cross-section is conveyed in Fig. 8c by an elliptical shape. This could reflect a molecular organization where the mesogens of a given column are non-uniformly distributed around the column axis.

(v) As in the Col_h phase, comparison of the length of the aromatic core ($\sim$23 Å) to the stacking distance ($\sim$11 Å) of the cubes within the columns of the Col_r phase suggests that mesogens belonging to adjacent cubes of the same column can, on average, interdigitate to one half of their length. The 2D packing of the columns corresponds to the herringbone scheme shown in Fig. 8c. It is apparent from this scheme that, although the mesogenic side-groups within a column are not uniformly distributed around its axis, the arrangement of mesogens in adjacent columns produces a more uniform mesogenic density-distribution around a given column axis as a result of the alternating orientations of the columns implied by the *p2gg* symmetry of the phase. Finally, notable is the fact that no peak analogous to peak E of the Col_h phase is observed in the Col_r phase. Thus, no apparent tilt angle is experimentally identified.

Within the above molecular model, the columnar–columnar phase transition is attributed to the rearrangement of the mesogenic units decorating the central silsesquioxane cube of the octapode. In other words, the phase transition here is associated with conformational changes. This is in accordance with the DSC observations of weak and broad exotherms and also with the polarizing microscopy experiments, where no considerable changes were observed in the patterns of the two phases. An analogous Col_h–Col_r phase transition,[25] albeit in a low molar mass calamitic system, has been reported to be second-order and was attributed to changes in the effective shape of the mesogens.

Table 6 Molecular data for pure compounds and binary mixtures

Substance	$\langle n \rangle$	$M_{mesogen}$/g mol^{-1}	M_{sp+c}/g mol^{-1}	M/g mol^{-1}
C-8B	8	5328	2256	7584
B÷**C-8B** (x = 0.84)	9.47	6307	2357	8664
B÷**C-8B** (x = 0.69)	11.44	7619	2493	10112
B÷**C-8B** (x = 0.44)	18.32	12201	2968	15169
B	—	666	69	735

Finally, it is worth contrasting the nematic and columnar ordering of the calamitic octapodes of the present study to the self organization (bilayer lamellas sandwiched between crystalline lamellas) recently observed in supermolecular structures consisting of silsesquioxane cubes with covalently attached mesogenic units of the discotic type.[26]

Conclusions

Based on XRD, and supported by POM and DSC observations, our structural analysis of the liquid-crystalline phases of mesogenic silsesquioxane octapodes and of their mixtures with the corresponding monomer, revealed a phase polymorphism that includes, in decreasing temperature succession, (i) a nematic phase with strong cybotactic clustering, (ii) a columnar phase with hexagonal two-dimensional ordering of the columns and tilted cybotactic clustering, which is reported for the first time and (iii) a non-centered columnar rectangular phase of *p2gg* symmetry and no apparent tilting within the columns.

The molecular organization is driven by a microsegration of the inorganic and organic groups, with the central core formed by the siloxane parts (cube and spacers) and decorated in the periphery by the mesogenic units. A molecular packing model suggests that the columnar hexagonal to rectangular phase transition is accompanied by extensive conformational rearrangement of the mesogenic segments of the octapodes.

The addition of low molar mass mesogens leads to a destabilization of the columnar phases. This is associated with an increased separation of the silsesquioxanes situated in the centre of the columns. In particular, addition of mesogens into the columnar assemblies reduces the effect of microphase separation and changes the hydrocarbon content in the compositions, *i.e.* modifies both of the factors that are responsible for the formation of the columnar phases.

Appendix 1: definition of binary mixture concentration

The concentration x is defined as the ratio of the number of mesogenic side-groups assembled into octapodes over the total number of mesogenic units in the mixture *i.e.*

$$x = \frac{8N_{C-8B}}{8N_{C-8B} + N_B}, \qquad \text{(A1.1)}$$

where $N_{C\text{-}8B}$ denotes the number of octapode molecules and N_B denotes the number of mesogenic ("free") monomers in the mixture.

With $M_{C\text{-}8B}$, M_B denoting the molar masses of the octapode **C-8B** and monomer **B** compounds, respectively, and with $m_{C\text{-}8B}$, m_B denoting the respective masses of these compounds in the mixture, the concentration x in eqn (A1.1) is given by:

$$x = \left(1 + \frac{m_B M_{C-8B}}{8 m_{C-8B} M_B}\right)^{-1}. \qquad \text{(A1.2)}$$

Appendix 2: determination of the transition enthalpies

The transition enthalpies in kJ mol^{-1} are calculated using:

$$\Delta H[\text{kJ mol}^{-1}] = \Delta H[\text{J g}^{-1}] \times M[\text{g mol}^{-1}]/1000, \qquad \text{(A2.1)}$$

where ΔH [J g^{-1}] is the experimentally determined transition enthalpy and M is the molar mass given in Table 6. In this Table, $M_{mesogen}$ represents the contribution of the mesogenic side-groups to the molar mass and M_{sp+c} represents the contribution of the spacers together with the silsesquioxane cube. For the **C-8B** compound and its mixtures, $\langle n \rangle$ denotes the average number of mesogenic units per silsesquioxane cube in the system. This is introduced in order to evaluate the separate contributions from $M_{mesogen}$ and M_{sp+c}. Finally, M denotes the total molar mass per silsesquioxane cube in the substance.

Acknowledgements

P. K. K. acknowledges financial support from the "Pythagoras" programme of the Hellenic Ministry of Education and the EU for a Marie Curie fellowship in the MC Training Site Project (HPMT-CT2001-00322).

References

1 V. Percec and M. Kawasumi, *Macromolecules*, 1992, **25**, 3843–3850.
2 F. L. Chen, A. M. Jamieson, M. Kawasumi and V. Percec, *J. Polym. Sci., Part B: Polym. Phys.*, 1995, **33**, 1213–1223.
3 V. Percec, P. Chu, G. Ungar and J. Zhou, *J. Am. Chem. Soc.*, 1995, **117**, 11441–11454.
4 S. Lecommandoux, M. F. Achard and F. Hardouin, *Liq. Cryst.*, 1998, **25**, 85–94.
5 M. Marcos, R. Giménez, J. L. Serrano, B. Donnio, B. Heinrich and D. Guillon, *Chem.–Eur. J.*, 2001, **7**, 1006–1013.
6 J. Barberá, B. Donnio, R. Giménez, D. Guillon, M. Marcos, A. Omenat and J. L. Serrano, *J. Mater. Chem.*, 2001, **11**, 2808–2813.
7 M. Saez, J. W. Goodby and R. M. Richardson, *Chem.–Eur. J.*, 2001, **7**, 2758–2764.
8 V. Percec, M. Glodde, M. Peterca, A. Rapp, I. Schnell, H. W. Spiess, T. K. Bera, Y. Miura, V. S. K. Balagurusamy, E. Aqad and P. A. Heiney, *Chem.–Eur. J.*, 2006, **12**, 6298–6314.
9 A. G. Vanakaras and D. J. Photinos, *J. Mater. Chem.*, 2001, **11**, 2832–2838.
10 C. Tschierske, *J. Mater. Chem.*, 2001, **11**, 2647–2671; B. Chen, X. B. Zeng, U. Baumeister, G. Ungar and C. Tschierske, *Science*, 2005, **307**, 96–99; B. Chen, U. Baumeister, G. Pelzl, M. K. Das,

X. B. Zeng, G. Ungar and C. Tschierske, *J. Am. Chem. Soc.*, 2005, **127**, 16578–16591.
11 A. Kohlmeier, D. Janietz and S. Diele, *Chem. Mater.*, 2006, **18**, 1483–1489.
12 B. Donnio, J. Barberá, R. Giménez, D. Guillon, M. Marcos and J. L. Serrano, *Macromolecules*, 2002, **35**, 370–381.
13 A. G. Vanakaras and D. J. Photinos, *J. Mater. Chem.*, 2005, **15**, 2002–2012.
14 M. Marcos, A. Omenat and J. L. Serrano, *C. R. Chim.*, 2003, **6**, 947–957.
15 K. Merkel, A. Kocot, J. K. Vij, R. Korlacki, G. H. Mehl and T. Meyer, *Phys. Rev. Lett.*, 2004, **93**, 237801; K. Neupane, S. W. Kang, S. Sharma, D. Carney, T. Meyer, G. H. Mehl, D. W. Allender, Satyendra Kumar and S. Sprunt, *Phys. Rev. Lett.*, 2006, **97**, 207802; D. Filip, C. Cruz, P. J. Sebastão, A. C. Ribeiro, M. Vilfan, T. Meyer, P. H. J. Kouwer and G. H. Mehl, *Phys. Rev. E: Stat. Phys., Plasmas, Fluids, Relat. Interdiscip. Top.*, 2007, **75**, 011704.
16 G. H. Mehl and I. M. Saez, *Appl. Organomet. Chem.*, 1999, **13**, 261–272; R. M. Laine, *J. Mater. Chem.*, 2005, **15**, 3725–3744.
17 S. Diez, D. A. Dunmur, M. R. De la Fuente, P. K. Karahaliou, G. Mehl, T. Meyer, M. A. Perez Jubindo and D. J. Photinos, *Liq. Cryst.*, 2003, **30**, 1021–1030.
18 R. Elsäßer, G. H. Mehl, J. W. Goodby and D. J. Photinos, *Chem. Commun.*, 2000, 851–852.
19 R. Elsäßer, D. Rodriguez-Martin, R. M. Richardson, D. J. Photinos, M. Veith, J. W. Goodby and G. H. Mehl, *2nd Anglo-Japanese Meeting on Liquid Crystals*, York, 2001; R. Elsäßer, D. Rodriguez-Martin, R. M. Richardson, D. J. Photinos, M. Veith, J. W. Goodby and G. H. Mehl, *Mol. Cryst. Liq. Cryst.*, 2003, **402**, 237–243.
20 A. De Vries, *Mol. Cryst. Liq. Cryst.*, 1970, **10**, 219.
21 O. Francescangeli, M. Laus and G. Galli, *Phys. Rev. E: Stat. Phys., Plasmas, Fluids, Relat. Interdiscip. Top.*, 1997, **55**, 481–487.
22 M. F. Achard, S. Lecommandoux and F. Hardouin, *Liq. Cryst.*, 1995, **19**, 581–587.
23 J. M. Montornes, J. A. Reina and J. C. Ronda, *J. Polym. Sci., Part A: Polym. Chem.*, 2004, **42**, 3002–3012.
24 S. Stojadinovic, A. Adorjan, S. Sprunt, H. Sawade and A. Jakli, *Phys. Rev. E: Stat. Phys., Plasmas, Fluids, Relat. Interdiscip. Top.*, 2002, **66**, 060701.
25 B. Donnio, B. Heinrich, H. Allouchi, J. Kain, S. Diele, D. Guillon and D. W. Bruce, *J. Am. Chem. Soc.*, 2004, **126**, 15258–15268.
26 L. Cui, J. P. Collet, G. Xu and L. Zhu, *Chem. Mater.*, 2006, **18**, 3503–3512.